Available online at www.sciencedirect.com

ScienceDirect

IFAC Papers Online CONFERENCE PAPER ARCHIVE

IFAC PapersOnLine 56-2 (2023) 10740–10745

Active and Data-driven Health and Usage Monitoring of Aircraft Brakes

José Joaquín Mendoza Lopetegui * **Gianluca Papa** * **Mara Tanelli** *

* *Dipartimento di Elettronica, Informazione e Bioingegneria, Politecnico di Milano, 20133 Milan, Italy, (e-mails: josejoaquin.mendoza@polimi.it; gianluca.papa@polimi.it; mara.tanelli@polimi.it)*

Abstract: Aircraft brakes are a safety-critical subsystem, and their prolonged use in each landing maneuver makes them subject to significant wear. Thus, it is crucial to devise efficient methods for monitoring their correct functioning and their health and usage status using the signals available in the Brake Control Unit. This paper proposes and validates an innovative data-driven approach to this problem. The proposed architecture is integrated with the Anti-lock Braking System algorithm providing combined health monitoring and anomaly detection for aircraft brakes in addition to an online estimate of the residual useful life of these components.

Keywords: Aircraft; anomaly detection; braking systems; health and usage monitoring; machine-learning

1. INTRODUCTION

Prognostics and Health Management systems in aeronautics can be traced back to the 1980s by the development of *Health and Usage Monitoring Systems* (HUMS) for helicopters. The early interest in the industry can be explained due to the efforts to reduce the high maintenance costs involved. Some civil aerospace studies show that maintenance activities can account for as much as 20% of an operator's direct operating costs, and line mechanics can spend 30% of their time trying to access information to diagnose failures, see Ferreiro et al. (2012). Different works can be found in the literature related to the development of health assessment methods intended for a wide variety of aircraft components. Some examples can be appreciated in Li et al. (2018) and Ordóñez et al. (2019). A particularly relevant aircraft subsystem in need of appropriate health assessment is the landing gear. An aircraft landing gear is designed to sustain the aircraft weight while providing adequate contact to the ground during landing, taxiing, and take-off type maneuvers, and failures during operation can result in catastrophic and dangerous conditions. As most landing gear health monitoring techniques still rely mostly on visual inspections and routine maintenance, there is a significant need for automatic methods that diagnose and predict landing gear health. Among the landing gear components, the braking system is the most subject to wear. Due to the mechanism by which the braking force is generated, the brake pads are the main component needing frequent maintenance and replacement. Moreover, braking maneuvers in aircraft, during landings or rejected take-offs (RTOs), have a significant duration and the Anti-lock Braking System (ABS) is always active, causing an elevated degradation of both tire and brakes, see D'Avico et al. (2021). It is thus of particular importance to devise efficient and applicable methods for the active monitoring of aircraft brakes, which can both detect abnormal behaviors and track the slower degradation dynamics, possibly indicating the residual useful life (RUL) of these components. Recently, these kinds of systems have received considerable attention in the prognostics and health management community. See the works by Oikonomou et al. (2022), Hsu et al. (2022), and Lee et al. (2022).

To this end, in this paper we propose a data-driven approach to this task, designing a combined anomaly detection and usage monitoring system that can be fully integrated with the ABS architecture. To be applicable, this system uses only the signals available on commercial Brake Control Units (BCUs), i.e., the wheel rotational speed and the pressure measurements. Starting from these signals, the brake usage is linked to the braking torque estimation problem, and a method based on statistical tests conducted on a Gaussian Mixture Model (GMM) is introduced to update the component RUL and detect anomalous conditions of the braking actuator. The proposed approach is tested in different braking conditions with both healthy and faulty braking system settings, and its performance is successfully tested on a detailed and validated aircraft simulator. To the best of the Authors' knowledge, such a combined active health monitoring and anomaly detection system integrated with the ABS algorithm is not available for aircraft brakes, and each specific functionality offers advances in itself.

The rest of the paper is organized as follows. Section 2 introduces the simulation model and its validation on experimental data. Section 3 presents the system architecture, detailing the design of each subsystem. Section 4 illustrates the obtained results and discusses its performance. Finally, Section 5 provides some closing remarks.

2. LANDING GEAR MULTIBODY SIMULATION SETTING

The simulation platform defined in this work is a single-wheel rigid body model representation of a trainer aircraft equipped with a tricycle landing gear. This type of model is a standard representation that captures the longitudinal dynamics involved in the braking actuator degradation process. Relevant phenomena encountered during on-ground braking maneuvers, such as vertical load variation, tire deflection, runway friction characteristics, and braking actuator dynamics have been modeled. The proposed

10.1016/j.ifacol.2023.10.735

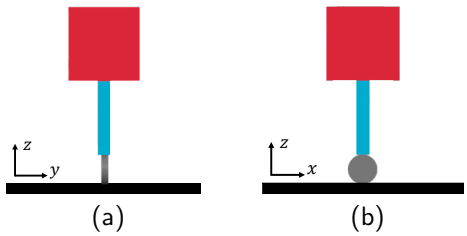

Fig. 1. Single-wheel rigid body model geometry. Left: Front view. Right: Lateral view.

simulation platform was implemented in the MATLAB-Simulink Simscape Multibody environment.

2.1 Longitudinal Dynamics

The single-wheel rigid body model is presented in Fig. 1. The equivalent aircraft body perceived by the wheel is represented by a single rigid body with mass m_a depending on the selected payload. In turn, the wheel is represented by a rigid body with mass m_w, rotational inertia J_w, and nominal radius $\bar{r}$ selected according to the manufacturer's specifications. The tire compression and the increase in contact surface are modeled indirectly by allowing the wheel-tire rigid body to penetrate the runway using a linear stiffness and damping reaction force. The wheel turns at a rotational speed ω while the system moves in the longitudinal plane with a linear velocity v_a. To brake, a torque T_b is available at the wheel rotational joint, which produces a force F_x to be exchanged at the tire-runway interface. As the study considers motions along the longitudinal plane, it is assumed that the lateral forces at the contact patch can be neglected so that F_x is:

$$F_x = F_x\left(F_z^w, \lambda\right), \tag{1}$$

where F_z^w describes the equivalent vertical load experienced by the tire, and λ refers to the longitudinal wheel slip. The vertical load F_z^w is approximated by computing $m_a g$ and subtracting the instantaneous lift force, where g is the gravity acceleration. The longitudinal wheel slip λ for a braking maneuver is defined as:

$$\lambda = 1 - \omega r(F_z)/v_a, \tag{2}$$

where $r(F_z)$ is the loaded wheel radius. As indicated by (2), $\lambda \in [0, 1]$, with $\lambda = 0$ representing the free-rolling condition and $\lambda = 1$ the locked-wheel condition. The functional relationship (1) was computed by employing the Fiala Model as presented in Pacejka (2012), by neglecting the camber angle contribution. The longitudinal friction coefficient μ between the ground and the tire has been characterized by the Burckhardt model from Burckhardt (1993). The analytical relationship is expressed as follows:

$$\mu(\lambda) = \theta_1\left(1 - e^{-\lambda\theta_2}\right) - \lambda\theta_3, \tag{3}$$

where θ_1, θ_2, and θ_3 are parameters that depend on the runway and tire condition. To explore a wide range of scenarios, eight different friction conditions identified from experimental data were selected. A frontal aerodynamic drag force is also considered. The expressions of the lift and drag forces are expressed as:

$$F_{drag/lift}(v_a) = (1/2)\rho v_a^2 S_{d/l} C_{d/l}, \tag{4}$$

with ρ the air mass density, $S_{d/l}$ the appropriate reference area, and $C_{d/l}$ the drag or lift coefficient, extracted from experimental data. Finally, the residual thrust from the aircraft engine is also considered a longitudinal force, computed as a velocity-dependent map.

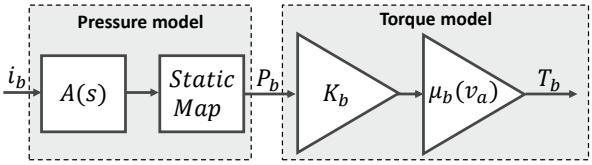

Fig. 2. Actuator model scheme. The input is the braking current i_b and the output is the braking torque T_b.

Table 1. Braking maneuver data

CONFIG	**mass** kg	**initial speed** m/s
Light landing	2800	49
Medium landing (a)	3150	52
Medium landing (b)	3300	53
Heavy landing	4450	61

2.2 Braking Actuator Nominal Model

The considered braking actuator uses electro-hydraulic servo valves to produce the braking torque T_b through the input of a current i_b. The torque generation happens as shown in Fig. 2. First, the input current i_b generates a pressure P_b by the hydraulic system in the chamber next to the disc brake, represented by a linear second-order dynamic model with delay $A(s)$ and a nonlinear gain dependent on the system operating condition, which have been experimentally identified. See D'Avico et al. (2018) for more details on the first conversion stage identification. Then, the pressure P_b generates a braking torque T_b by pressing a caliper endowed with a brake pad against the disc brake rotor, represented by a set of gains. The static portion of the conversion is modeled by a gain K_b which can be obtained by the manufacturer specifications. The dynamic portion of the conversion involves the effective value of the braking friction coefficient μ_b within each braking maneuver. In previous work by the Authors, three different characteristic behaviors of the braking friction coefficient with respect to the longitudinal aircraft speed were observed, associated with a particular aircraft payload configuration. The specific details of the landings are presented in Table 1. See Mendoza Lopetegui et al. (2022a) for more details on the second conversion stage.

2.3 Braking Actuator Wear

During the braking actuator lifetime, the component wear alters its properties, which affects its capabilities to produce braking torque, expressed as a variation of the average value of the braking friction coefficient μ_b. In Mendoza Lopetegui et al. (2022a), a progressive reduction of μ_b was observed so that the same braking pressure generates lower torque values as usage increases. For this reason, the value of μ_b along with its trend after multiple consecutive maneuvers reflects the status of the braking actuator, which is related to the cumulative braking energy that the actuator has released. In Mendoza Lopetegui et al. (2022a), a probabilistic modeling approach proved useful in capturing the evolution of the component wear trajectory. The tool employed was a Gaussian Mixture Model (GMM) with four components, briefly recalled next. A GMM describes a probability distribution as a weighted sum of M mixture components, each being a normal probability distribution with a certain weight $w_i \in (0, 1)$. The probability density $p(x|\phi)$ of the GMM will read

$$\begin{cases} p(x|\phi) = \sum_{i=1}^{M} w_i \frac{e^{-\frac{1}{2}(x-\mu_i)^T \sigma_i^{-1}(x-\mu_i)}}{\sqrt{(2\pi)^k det(\sigma_i)}} \\ \sum_{i=1}^{M} w_i = 1 \end{cases} \tag{5}$$

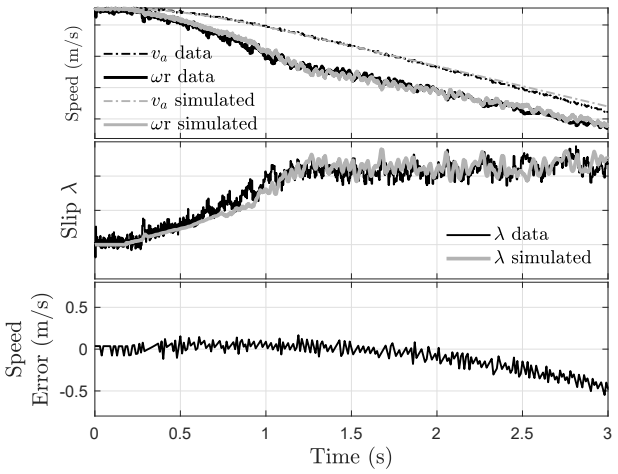

Fig. 3. Validation test of the model. Top and middle plot: Measured and simulated wheel speed, body speed, and wheel slip. Bottom plot: velocity estimation error.

where σ_i is the covariance matrix of the i-th component, μ_i is the mean vector of the i-th component, x is the vector of regressors and $\phi = [\mu_1, \sigma_1, \ldots, \mu_M, \sigma_M]$ is the vector of parameters. The vector of regressors x was chosen to be composed of the cumulative energy dissipated by the disc brake c_e and the mean disc brake friction coefficient $\bar{\mu}_b$ across a braking maneuver as $x^T = [c_e \ \bar{\mu}_b]$.

2.4 Anti-skid Controller

To conduct braking maneuvers in the simulator, a longitudinal slip-based anti-skid controller was designed. Its task was to safely bring the aircraft to a standstill while avoiding wheel-locking events for the whole range of maneuvers from Table 1 over the eight friction conditions mentioned in Section 2.1. The slip-based controller is formulated as a tracking control problem of the longitudinal slip λ to a selected reference $\overline{\lambda}$. The designed controller provides as output a current value i_b, which is converted into the braking torque T_b by the actuator, and applied to the system. A Proportional Integral Derivative (PID) structure has been selected for the wheel slip controller and we refer the reader to Mendoza Lopetegui et al. (2022a) for details about the controller design, tuning, and robust performance on a standard set of braking maneuvers.

2.5 Simulation Framework Validation

The proposed simulation environment has been validated in braking maneuver scenarios to check for the replication of available experimental measurements of braking maneuvers performed with a flywheel test rig. The results obtained in one of the validation scenarios will be presented. The validation scenario corresponds to a landing maneuver performed at Light landing conditions with medium runway friction. The results of the test are presented in Fig. 3 with the numerical values of the vertical axes removed as they contain confidential experimental data. In Fig. 3, a comparison between the experimental and simulated aircraft velocity v_a, wheel speed ω, and longitudinal slip λ is shown; while the bottom plot shows the prediction error of the aircraft longitudinal velocity v_a. The obtained results confirm the simulator's capabilities to predict accurately the longitudinal quantities relevant to study the braking actuator degradation.

3. PROPOSED SYSTEM ARCHITECTURE

The proposed monitoring system is shown in Fig. 4: it is composed of three main blocks: Health Monitoring, Estimation, and Anomaly Detection. The Health Monitoring block calculates the RUL based on a physics-based wear model fed by the only two measurements available in the Brake Control Unit: pressure P_b and wheel speed ω. The Estimation block estimates the applied braking torque $\hat{T}_b$, the dissipated braking energy $\hat{E}_b$, and the braking friction coefficient $\hat{\mu}_b$ through a Proportional Integral Observer. In the Anomaly Detection block, the estimated output quantities $\hat{E}_b$ and $\hat{\mu}_b$ are compared through a hypothesis test against the expected system evolution as described by a GMM. The final system output is a report about the landing gear status after each maneuver, consisting of the RUL, the estimated braking energy, the estimated braking friction coefficient, and a warning if the system is behaving in an anomalous manner. In the following subsections, each block is described in detail.

3.1 Health Monitoring: RUL Estimation

This block estimates the RUL of the braking actuator. The block output is a percentage between 0% to 100%, with 100% corresponding to a brand-new actuator. For this, the block relies on the applied pressure P_b and wheel speed ω. As the component of the braking actuator subject to most of the wear is the brake pad material, it is natural to seek a RUL metric related to the removed material from the brake pads. Hence, a direct relationship between the material consumed by the brake pads with respect to P_b and ω is desirable. The most widely used approach to capture this phenomenon was presented in Archard (1953), in which the wear is described as proportional to the load and the sliding distance. The Archard law is commonly used in related engineering applications as pointed out in Zmitrowicz (2006), being the preferred choice for this work as well. The basic version of the law can be expressed as:

$$\Delta V = \left(K F_N(t) \Delta s_\lambda\right) / H, \tag{6}$$

where ΔV is the volume of wear debris removed from the component, K is a non-dimensional wear coefficient, F_N is the normal load, Δs_λ is the sliding distance between the surfaces and H is the hardness of the softer contact surface. Rewriting the equation by normalizing by the contact area A and defining $\kappa = \frac{K}{H}$, the law can be expressed as:

$$\Delta h = \kappa P_b(t) \Delta s_\lambda, \tag{7}$$

with Δh the wear depth of the material being worn down, κ a dimensional coefficient, and $P_b(t)$ the applied pressure. Expanding the sliding distance and dividing by the dimensional coefficient, a normalized wear metric can be formulated:

$$\Delta \gamma = P_b(t) \omega(t) R_{eff} \Delta t, \tag{8}$$

with $\Delta\gamma$ the quantity tracking the wear process, R_{eff} the brake pad effective radius at the contact point, ω the wheel speed and Δt the time elapsed. By accumulating (8) over time, the brake pad wear can be monitored by relying only on measurable signals of the BCU. In this way, if the previous quantity is computed on healthy specimens from a brand new condition up to the end of their useful life, the quantity γ can be identified. A limit called γ_f can be defined related to the required amount of material from the brake pads that can be removed before replacement of the component is needed, which can be extracted from the experimental data. Finally, to define a RUL metric, if the system calculates the current value of $\gamma(t)$ for the braking actuator at time t, the following index can be proposed:

$$\mathrm{RUL}(t) = \left(\gamma_f - \gamma(t)\right) / \gamma_f. \tag{9}$$

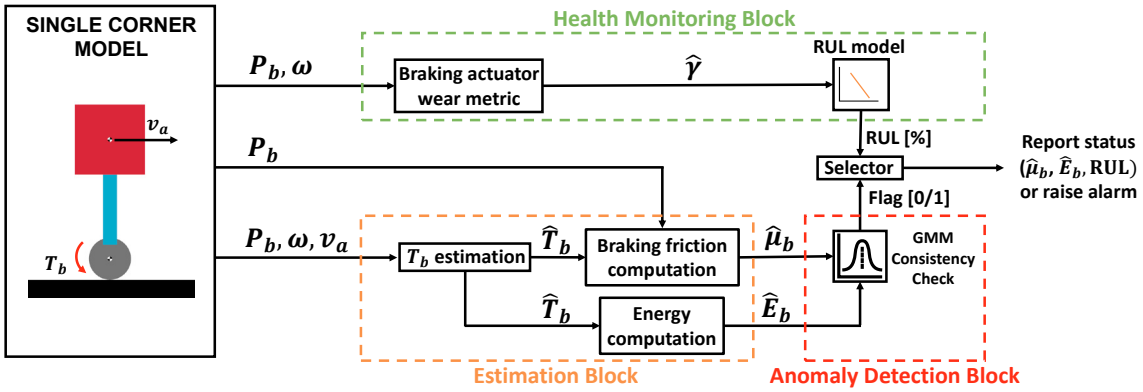

Fig. 4. Architecture of the proposed Health Monitoring and Anomaly Detection scheme. The three main blocks of the procedure are highlighted.

3.2 Estimation: Software Sensing of the Braking Torque

This block estimates the two variables used by the GMM to describe the system condition, which are inputs to the Anomaly Detection Block. Both the energy consumed by the brake pad E_b and the braking friction coefficient μ_b require the knowledge of the braking torque T_b. The construction of the GMM was conducted using real measurements from the torque T_b as part of an actuator characterization campaign with a specially constructed test bench. However, in normal operating conditions, the anti-skid only has access to the braking pressure. The torque estimation problem was described in detail in Mendoza Lopetegui et al. (2022b) along with a comparison of several approaches to construct a robust torque estimator. In this work, we leverage the results obtained in the previously mentioned work and use a Proportional Integral Observer for the Estimation block. Once the torque $\hat{T}_b$ has been estimated, the braking friction $\hat{\mu}_b$ can be computed:

$$\hat{\mu}_b(t) = \hat{T}_b(t)/(P_b(t)K_b). \tag{10}$$

The mean value $\bar{\mu}_b$ of $\hat{\mu}_b(t)$ during the maneuver will be the final procedure output. Finally, to compute the estimated energy consumed by the brake pads in a particular braking maneuver, it is enough to compute the braking actuator energy consumption, that is:

$$\hat{E}_b = \int_{t_1}^{t_2} \hat{T}_b(t)\omega(t)dt, \tag{11}$$

where t_1 and t_2 refer to the start and end of the braking maneuver, respectively.

3.3 Anomaly Detection: Consistency Check

The block detects possible anomalous conditions of the braking actuator and reports the component RUL. In particular, it outputs a binary flag set to 1 when the degradation rate of the component is not consistent with the nominal expected behavior, hence calling for maintenance. On the opposite, if the component degrades as expected, the block sets the binary flag to 0 and reports the RUL, along with the braking friction coefficient and cumulative consumed braking energy. The inputs to the block are the mean estimated value of the friction coefficient after each maneuver is finished $\bar{\mu}_b$, and the estimated amount of dissipated energy in the brake pads of that particular maneuver $\hat{E}_b$. The algorithm operates through four main steps, depicted in Fig. 5, and described next.

Step 1: Sliding Window This step collects the estimation pairs ($\bar{\mu}_b$,$\hat{c}_e$) that are derived from the Estimation Block after every landing and stores them in a window containing the last N pairs, where $\hat{c}_e$ is the estimated cumulative braking energy dissipated by the brake pads. The main parameter of this step is the number of stored points N. In other words, at time t, the window will be composed of those pairs, indexed by i, running from $t-N+1$ up to t:

$$(\bar{\mu}_b^i, \hat{c}_e^i) \in S(t), \forall i \in \{t-N+1, \ldots, t\}, \tag{12}$$

where the set $S(t)$ indicates the pairs belonging to the window at time t.

Step 2: Clustering This step classifies the window into one of the four components from the GMM of the nominal wear behavior as described in Section 2.3. To perform the classification, out of the N pairs composing the window, each pair i will be classified as one of the four GMM components, and the window will be assigned to one of them via a majority vote. The assignment of each pair i can be conducted by looking at the likelihood function for each of the four components and choosing the one which maximizes said index. In other words:

$$g_i = \underset{k=1}{\overset{4}{\operatorname{argmax}}} \left\{ \log\left(L((\bar{\mu}_b^i, \hat{c}_e^i)|\phi_k^*) \right) \right\}, \forall (\bar{\mu}_b^i, \hat{c}_e^i) \in S(t), \tag{13}$$

where $g_i \in \{1,2,3,4\}$ denotes the GMM component index that pair i in the window gets assigned to, $L((\cdot)|\phi_k^*)$ is the likelihood function of the two-dimensional Gaussian distribution of the GMM component $k \in \{1,2,3,4\}$ with parameters ϕ_k^*. Then, if the sliding window assignment index at time t is called $w(t) \in \{1,2,3,4\}$, the majority voting will proceed as:

$$w(t) = \underset{k=1}{\overset{4}{\operatorname{argmax}}} \left\{ \sum_{i=t-N+1}^{t} \left(g_i == k \right) \right\}, \tag{14}$$

where the operator == returns 1 if both operands are equal and 0 otherwise. Selecting N as an odd number simplifies the result of the majority voting procedure.

Step 3: Local Probability Density Once the window has been classified as the most likely GMM component, this step defines a local probability density allowing for a statistical test. The associated one-dimensional probability density conditioned to the observed cumulative braking energy $\hat{c}_e$ is extracted from the selected two-dimensional GMM component. In particular, the conditional probability is computed from the average cumulative energy $\bar{\hat{c}}_e(t)$ in the window of N samples, which is defined as:

$$\bar{\hat{c}}_e(t) = \left(\frac{1}{N} \right) \sum_{i=t-N+1}^{t} \left(\hat{c}_e^i \right), \tag{15}$$

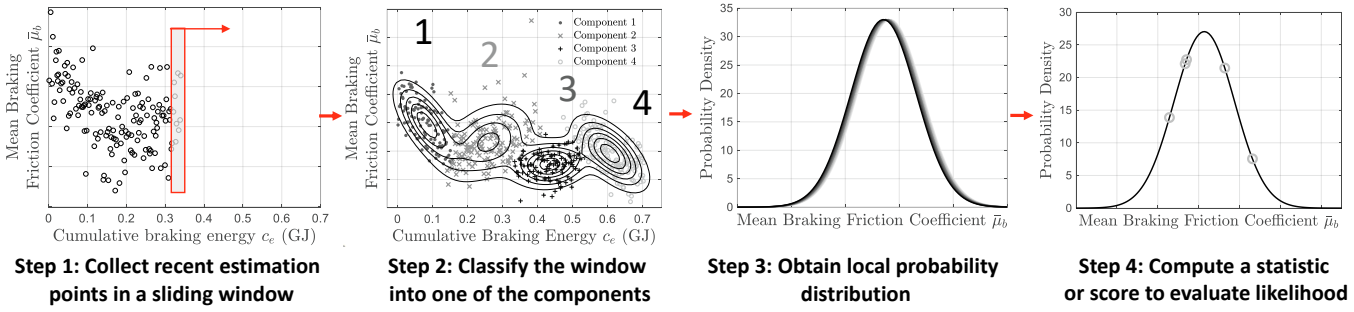

Fig. 5. Conceptual description of the four steps composing the Anomaly Detection Block.

from which the conditional probability density is:

$$P(\bar{\mu}_b|c_e = \bar{\hat{c}}_e(t)) \sim$$
$$N\Big(\bar{\mu}_b^j + \frac{\sigma_{\mu_b}^j}{\sigma_{c_e}^j}\rho^j(\bar{\hat{c}}_e(t) - \bar{\mu}_{c_e}^j), (1-(\rho^j)^2)(\sigma_{\mu_b}^j)^2\Big), j = w(t), \tag{16}$$

with ρ^j the correlation coefficient of the j-th GMM component; $\sigma_{\mu_b}^j$ and $\sigma_{c_e}^j$ the standard deviations of the j-th GMM component along the braking friction coefficient and cumulative braking energy axes, respectively; while $\bar{\mu}_b^j$ and $\bar{\mu}_{c_e}^j$ are the mean values of the j-th GMM component along the braking friction coefficient and cumulative braking energy axes, respectively.

Step 4: Statistical Test To determine if the data from the set $S(t)$ fits the local distribution, a statistical test is performed on the obtained local one-dimensional Gaussian probability density. A Z-test with an associated significance level p is used to evaluate the null hypothesis, defined as the assumption that the observed data does indeed come from a Gaussian density with given mean and standard deviation $P(\bar{\mu}_b|c_e = \bar{\hat{c}}_e(t))$, as calculated from the previous step in (16). By redefining the expressions of the conditioned mean and standard deviation from (16) right-hand side as $\tilde{\mu}$ and $\tilde{\sigma}$, and by considering the observed mean of the regressors in the window of length N as $\bar{\tilde{x}}$, the Z-score can be computed as $Z = (\bar{\tilde{x}} - \tilde{\mu}) \,/\, \left(\tilde{\sigma}\sqrt{N}\right)$.

The result of the statistical test will be either a rejection of the null hypothesis, so that evidence does exist to cast doubt on the observed monitored window, hence suggesting an anomaly in the wearing behavior; or a failure to reject the null hypothesis, so that no evidence exists to produce a judgment. A relationship exists between the significance level p and the number of samples in a window N. A possible way to choose them is to resort to the Power of the test. In this scenario, it quantifies the probability of flagging correctly the window as anomalous. A Power level of 99% was specified, with a detectable distance of 0.051 units of mean friction coefficient and a significance level of $p = 0.001\%$. For the statistical test considered, under the previous constraints specified, the minimum amount of samples N required for the window can be derived and corresponds to $N = 3$. Once the assessment of a particular window is completed, the system will either report the RUL if no evidence exists to suggest an anomaly or flag the window as anomalous if the window failed the Z-test, sending a warning to call for inspections.

4. METHOD EVALUATION

In this section, the proposed method is evaluated by applying the pipeline in sets of braking maneuvers obtained through the simulator described in Section 2. Two scenarios are considered: A braking actuator in nominal conditions and a braking actuator subjected to an accelerated wear rate.

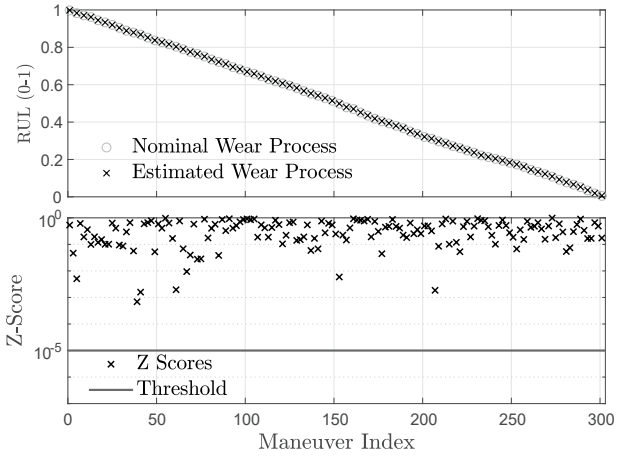

Fig. 6. Results with a nominal wear profile. Top: Comparison between the simulated and estimated RUL of the actuator during the 303 maneuvers. Bottom: Corresponding Z-Scores.

4.1 Data Set and Experiment Description

To evaluate the method performance on representative scenarios, the runway condition and aircraft inertial configuration variability were taken into account. More precisely, all the runway conditions mentioned in Section 2.1, as well as the four aircraft configurations from Table 1 were considered. In this manner, by combining the eight friction curves with the four aircraft configurations, a pool of 32 possible scenarios were constructed. From the pool, random scenarios were selected and performed in sequence with the simulation environment, subjecting the actuator to progressive wear as the experiment was conducted. The braking actuator was initialized as brand new and the experiment was stopped when the brake pad surface wear variable γ reached the threshold γ_f, as identified from the experimental data, considering the situation as the end of the component useful life.

4.2 Scenario 1: Nominal Actuator Behavior

In this scenario, the system was left to evolve considering the nominal wear process described in Section 2.3. In this manner, the braking actuator emulates the behavior of a healthy specimen during its lifetime. Under this scenario, an adequate health monitoring and anomaly detection system would refrain from flagging anomalies, minimizing

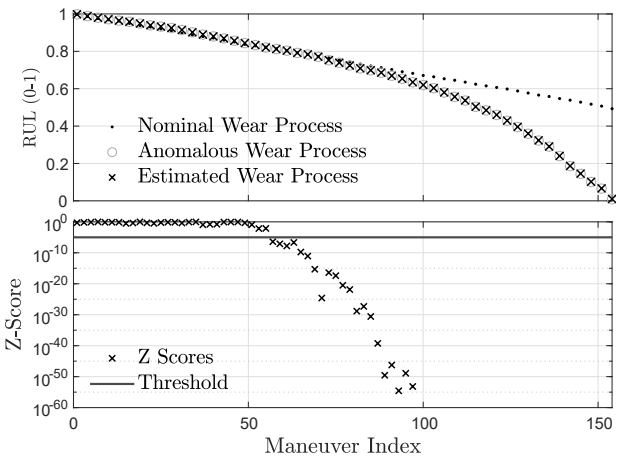

Fig. 7. Results with anomalous wear profile. Top: Comparison between the simulated and estimated RUL in the 154 maneuvers. Bottom: Corresponding Z-Scores.

thus unnecessary inspections, while tracking the braking actuator wear. In this case, it took the braking actuator 303 braking maneuvers to get to fully worn status. The results of the proposed methodology are reported in Fig. 6. As seen from the top section of Fig. 6, the RUL evolution is correctly tracked by relying on the measurements of P_b and ω. In the bottom part of Fig. 6, the results from the Anomaly Detection Block are reported. It can be observed that no window is reported as anomalous, and the Z-Scores yield values consistently above the proposed threshold. Hence, the RUL estimations shown in Fig. 6 will be correctly reported to the user by the system.

4.3 Scenario 2: Faulty Actuator Behavior

The second scenario considers an anomalous actuator. The anomaly starts after the 50^{th} maneuver and is simulated by accelerating the wear rate of the actuator, hence decreasing the friction coefficient μ_b value at the start of each maneuver. This scenario represents an actuator that is excessively losing material and braking capability. In this case, it took the braking actuator 154 braking maneuvers to wear down all the material. The results of the proposed methodology are reported in Fig. 7. Focusing on the top part of Fig. 7, a correct tracking of the RUL evolution is observed. For ease of comparison, also the nominal actuator behavior from Scenario 1 is overlaid, where the difference between the wear characteristics is evident. In the bottom part of Fig. 7, the results from the Anomaly Detection Block are reported. It can be observed that starting from maneuver 57, all subsequent windows are flagged as anomalous, as the system correctly detects an inconsistency between the cumulative braking energy absorbed by the brake pads and the observed friction coefficient, and calls for extraordinary component inspection.

5. CONCLUSION

In this paper, an innovative health monitoring scheme for aircraft brakes has been proposed. Specifically, we showed that a reliable and robust solution, which uses the only information available at the Brake Control Unit, i.e., braking pressure and wheel rotational speed, can be designed. The proposed approach encompasses several subsystems that deal with torque estimation, anomaly detection of potential abnormal behaviors, and the estimation of the health status of the component updated after each maneuver. The results obtained on a detailed and validated simulator are promising, showing high accuracy in estimating the braking actuator's residual useful life and detecting nominal or faulty behavior. As a future development, the scheme implementation in a braking system test rig is contemplated, as well as the integration of the method with an anti-skid algorithm to improve braking performance.

REFERENCES

Archard, J.F. (1953). Contact and rubbing of flat surfaces. *J. Appl. Phys.*, 24(8), 981–988. doi:10.1063/1.1721448.

Burckhardt, M. (1993). *Fahrwerktechnik: Radschlupf-Regelsysteme (Chassis technology: Wheel slip control systems)*. Vogel Verlag, Wüzburg, Germany. ISBN 978-3-80-230477-4.

D'Avico, L., Tanelli, M., and Savaresi, S.M. (2018). Experimental validation of landing-gear dynamics for anti-skid control design. In *2018 Eur. Control Conf. (ECC)*, 2751–2756. doi:10.23919/ECC.2018.8550258.

D'Avico, L., Tanelli, M., and Savaresi, S.M. (2021). Tire-wear control in aircraft via active braking. *IEEE Trans. Control Syst. Technol.*, 29(3), 984–995. doi:10.1109/TCST.2020.2983375.

Ferreiro, S., Arnaiz, A., Sierra, B., and Irigoien, I. (2012). Application of bayesian networks in prognostics for a new integrated vehicle health management concept. *Expert Syst. Appl.*, 39, 6402–6418. doi:10.1016/j.eswa.2011.12.027.

Hsu, T.H., Chang, Y.J., Hsu, H.K., Chen, T.T., and Hwang, P.W. (2022). Predicting the remaining useful life of landing gear with prognostics and health management (phm). *Aerospace*, 9(8). doi:10.3390/aerospace9080462.

Lee, J., Mitici, M.A., Geng, S., and Yang, M. (2022). Designing reliable, data-driven maintenance for aircraft systems with applications to the aircraft landing gear brakes. In *Proc. 32nd Eur. Saf. Reliab. Conf.* (ESREL 2022).

Li, T., Wang, S., Shi, J., and Ma, Z. (2018). An adaptive-order particle filter for remaining useful life prediction of aviation piston pumps. *Chinese J. Aeronaut.*, 31(5), 941–948. doi:10.1016/j.cja.2017.09.002.

Mendoza Lopetegui, J.J., Papa, G., Morandini, M., and Tanelli, M. (2022a). Data-driven modeling and regulation of aircraft brakes degradation via antiskid controllers. *IEEE Trans. Reliab.*, 1–11. doi:10.1109/TR.2022.3194646.

Mendoza Lopetegui, J.J., Papa, G., Tanelli, M., and Savaresi, S.M. (2022b). Comparing braking torque estimation approaches for active health monitoring of braking systems in aircraft. In *2022 IEEE Conf. Control Technol. Appl. (CCTA)*, 267–272. doi:10.1109/CCTA49430.2022.9966063.

Oikonomou, A., Eleftheroglou, N., Freeman, F., Loutas, T., and Zarouchas, D. (2022). Remaining useful life prognosis of aircraft brakes. *Int. J. Progn. Health Manag.*, 13(1). doi:10.36001/ijphm.2022.v13i1.3072.

Ordóñez, C., Sánchez Lasheras, F., Roca-Pardiñas, J., and de Cos Juez, F.J. (2019). A hybrid arima-svm model for the study of the remaining useful life of aircraft engines. *J. Comput. Appl. Math.*, 346, 184–191. doi:10.1016/j.cam.2018.07.008.

Pacejka, H.B. (2012). *Tire and Vehicle Dynamics, 3rd edition*. Butterworth-Heinemann. doi:10.1016/C2010-0-68548-8. ISBN 978-0-08-097016-5.

Zmitrowicz, A. (2006). Wear patterns and laws of wear – a review. *J. Theor. Appl. Mech.*, 44, 219–253.